Flexural impact response of textile reinforced cementitious composites (TRC)

Jan Wastiels[a]*, Johan Van Ackeren[a], Tine Tysmans[a], Wim Van Paepegem[b]

[a] Department of Mechanics of Materials and Constructions, Vrije Universiteit Brussel, Pleinlaan 2, 1050 Brussels, Belgium

[b] Department of Materials Science and Engineering, Ghent University, Belgium

*Corresponding author: Tel: +32 2 6292840, E-mail jan.wastiels@vub.be

Keywords: impact behaviour, cement composites, high performance, glass fibres, textile reinforced cement, TRC

Abstract

This work presents the characterisation of the local low velocity impact behaviour of a high performance fibre reinforced cementitious composite (HPFRCC) made of phosphate cement and different types of E-glass textile reinforcements. The so called "energy profiling method" that was used for quantitative characterisation is adopted from

Liu et al. (2004) who introduced this methodology on polymer matrix composites (PMC). A series of plates reinforced with chopped strand E-glass fibre mats (fibre volume fraction of 24%) was impacted during drop weight tests, showing that this methodology is as well applicable to textile reinforced cementitious composites. Further, the effects of impactor size and plate thickness were investigated experimentally, and finally the obtained results were compared to literature data for polymer matrix composites.

1. Introduction

It is known from literature that laminated polymer matrix composite structures, eventually stiffened or in sandwich form, present superior specific energy absorption compared to their metallic counterparts. The different damage mechanisms such as delamination, fibre debonding, and fibre and matrix cracking, make them suitable candidates for high energy absorption applications such as protecting structures against low velocity impacts [1]. Besides the composite materials with polymer matrix (PMC), a new generation composites with a cementitious matrix has been developed during recent years, the so called High Performance Fibre Reinforced Cementitious Composites (HPFRCC). A definition for these cementitious composite materials was presented by Naaman and Reinhardt [2,3]. HPFRCC materials are characterised by their distinct tensile strain hardening behaviour which leads to an increased energy absorption capacity. Their characteristics can even be enhanced when making use of well-oriented and well-structured fibre textile reinforcement, as in textile reinforced cement or concrete (TRC) [4-7]. High tensile strength and post-cracking stiffness, as well as strict crack control, can be obtained with high volume fractions (over 20%) of different fibres (glass, carbon, aramid, ...) [8,9]. Some differences with polymer matrix composites can however be expected in the damage and failure mechanisms under impact loading: indeed, the cementitious matrix is stiffer but more brittle than most polymeric matrices, presenting a small failure strain in tension and shear; moreover, the bond strength between fibres and matrix is much lower. Several studies of TRC under dynamic tensile loading [10-12] or flexural impact loading [13-16] were published in recent years. They are however restricted to beam configurations, and the information on energy absorption capacity and damage mechanisms is limited.

Low velocity impact behaviour is often assessed using drop weight impact tests. Even though a standard ASTM impact test, describing a single drop weight impact test and its configuration, is available for polymer matrix composites (PMC) [17], it does not allow the complete and objective characterisation of the impact behaviour of the composite plate material in relation with the occurring damage. In this paper, it is investigated whether a testing and analysis methodology, originally developed for PMC, can be applied to TRC composites in order to quantitatively and objectively characterise and compare their low velocity impact behaviour.

This methodology, called the energy profiling technique, was developed by Liu [18,19], and allows to link the quantitative results to the observed damage phenomena. A total of around 10 to 15 identical plate specimens of the composite material of interest are manufactured. Each specimen is tested in a drop weight impact test at a different impact energy level. The force and displacement histories are measured during the complete impact event, and are used for the interpretation of the results with regard to the occurring damage phenomena. Essentially, the produced data are processed in order to obtain a “master curve” that contains all force-deflection curves of the tested plates, and a so called "energy profile" in which the absorbed energy for each test is compared to the impact energy as determined from the potential energy of the impactor before the test.

2. Experimental program

2.1. Test set-up

The used testing device is a drop weight tower which is schematically drawn in Figure 2, and which was developed at the Department of Materials Science and Engineering at the University of Ghent [20]. The drop weight tower consists of an impactor, sliding along two guiding bars which are supported horizontally against a wall. The roller bearings are designed in order to minimize friction along the sidebars. The level of impact blow can be varied by changing the drop height of the impactor, with a maximum height of 3 m. It can be noticed that this changes simultaneously both the impact energy and the impact velocity. The end part of the impactor can be equipped with a hemispherical head with a diameter according to the user's needs. In order to enable the evaluation of the effect of the impactor head diameter, two hemispherical heads are used in this work. Their respective diameters are 50 mm and 70 mm. Results for a head diameter of 20 mm were reported elsewhere, and will be used as comparison [21]. The total mass of the impactor is around 7.9 kg. The square plate specimens are clamped along their four edges within a 250 mm by 250 mm square steel frame. Homogeneous clamping is obtained using 20 bolts equally divided over the four edges. The bolts are screwed with a torque key to assure an equal tightening at all positions.

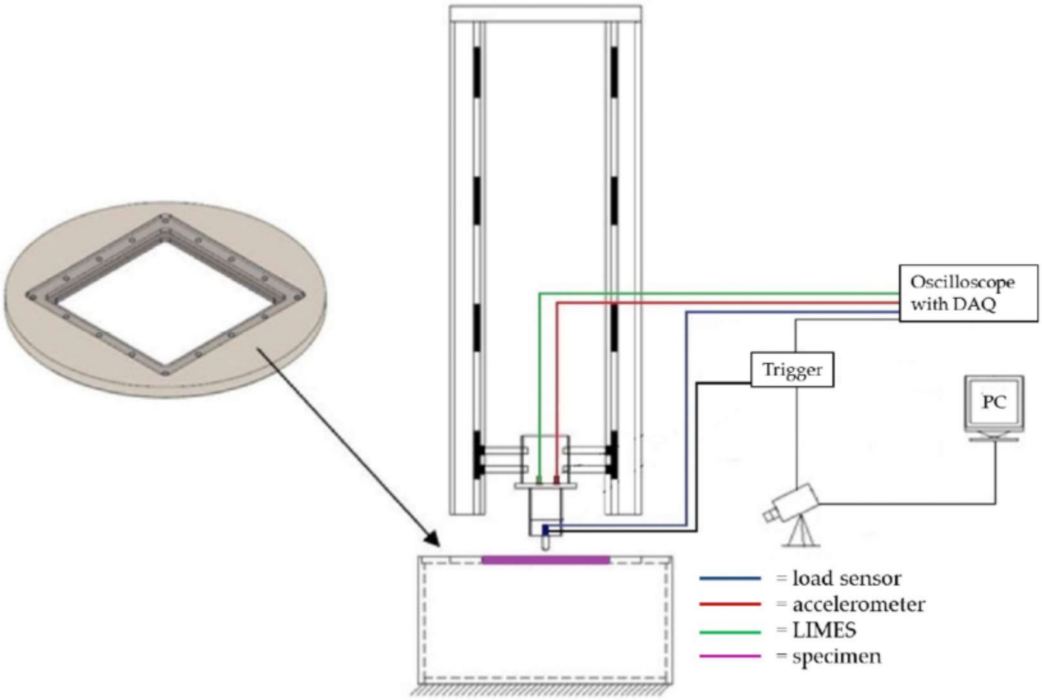

Figure 1: *drop weight impact test set-up*

As is shown in Figure 1, the set-up is equipped with three sensors which are all placed on the impactor. The load sensor (blue), Isotron type Endevco model 2311-1 with a full range of +22000/-2200 kN, is positioned as close as possible to the head of the impactor in order to avoid interference of joints and bolted parts. The acceleration sensor (red), an ICP Accelerometer model 350B03 with a full scale of ±10000 g, is placed on top of the impactor. The third sensor, which is indicated in green, is a magnetic displacement sensor Kübler Limes LI20/B1. The data obtained from this sensor were however not sufficiently accurate to measure the deflections. These were obtained by double integration over time of the acceleration signal, the accuracy of which was verified by comparison with digital image correlation measurements on the impactor.

Furthermore, all drop weight tests are recorded with a high speed camera (Photron APX-RS) which is placed in front of the impactor, providing a view on the plate during the impact event. The different damage mechanisms can be linked to the camera footage of the impact. The frame rate was limited to 4500 fps in order to ensure a maximum resolution of 1024x1024. The data measurements from the equipment on the impactor are synchronised with the data capturing of the camera. Triggering is performed based on a load threshold level of 200N. The total time window for the measurements is set to 3 seconds (0.5 s before, and 2.5 s after the trigger point), which is sufficiently long to capture the impact event.

2.2 Test series - specimens

Four series of at least 11 plate specimens are manufactured by means of hand lay-up as described in [22]. A constant fibre volume fraction V_f of 24% was targeted. Their characteristics (average and standard deviation) are given in Table 1.

Table 1: *overview of the test series*

series name	average thickness (mm)	average mass (kg)	V_f (%)	$\varnothing_i$ (mm)	h (mm)	max E_i (J)
CSM-20	4.01 (0.18)	503 (26)	23.7 (0.9)	20	50-1000	77.7
CSM-50	3.83 (0.11)	484 (18)	24.7 (0.7)	50	50-750	58.0
CSM-70	3.95 (0.06)	503 (9)	23.9 (0.4)	70	50-850	65.7
CSM-70-4	2.17 (0.11)	256 (14)	21.8 (1.1)	70	50-350	27.1

CSM in the name stands for the used reinforcement: emulsion bonded glass fibre chopped strand mat type M705 manufactured by European Owens Corning Fiberglas, with nominal mat weight of 300 g/m^2. The numbers 20, 50 and 70 in the name stand for the impactor diameter $\varnothing$ in mm. Each laminate is build up with 8 layers of fibre mat, except series CSM-70-4, which contains only 4 layers. The range of drop heights h, and the corresponding maximum impact energy E_i are also given in Table 1.

3. Results and discussion

In the first part of this section, the damage phenomena and damage mechanisms during a low velocity impact event on IPC-TRC composite plates are studied using the energy profiling method proposed by Liu [18,19], supported by the high speed camera images. Subsequently, the effect is investigated of changing test and specimen parameters on the impact characteristics. In the last part of this section, the obtained results for TRC are compared to results from literature obtained for PMC.

3.1 Damage characterisation

The data resulting from the impact tests are presented in Figures 3 to 6 and Tables 2 to 5 in the next section 3.2. In the present section, the general impact behaviour of IPC-TRC composite plates will be described, based on an excerpt of the data from series "CSM-20" (Figure 3), which is represented in Figure 2. The synchronisation of the camera footage (not represented here) with the test data is used to support the following observations:

- all force-deflection curves are quite similar in their ascending loading stage and descending unloading stage, except the rebounding stage (decreasing deflection in the unloading stage). As such, they form a mountain-shape master curve. The main damage in the plate occurs locally, even though the deflections of the plate can become relatively large;
- none of the force-deflection curves are returning to the origin after the impact, and are therefore not fully closed. This implies that for none of these impact events the energy absorption is fully elastic. Nevertheless, curves 1a and 1b of Figure 2 (low impact energies) could be considered as closed curves, because of their pronounced rebounding section and the small contribution of the matrix damage.

The absorbed energy for curves 1a and 1b remains less than half of the impact energy, and is resulting from local matrix indentation at the contact area and local debonding and slip between fibres and matrix. It is proposed to call this the indentation range;

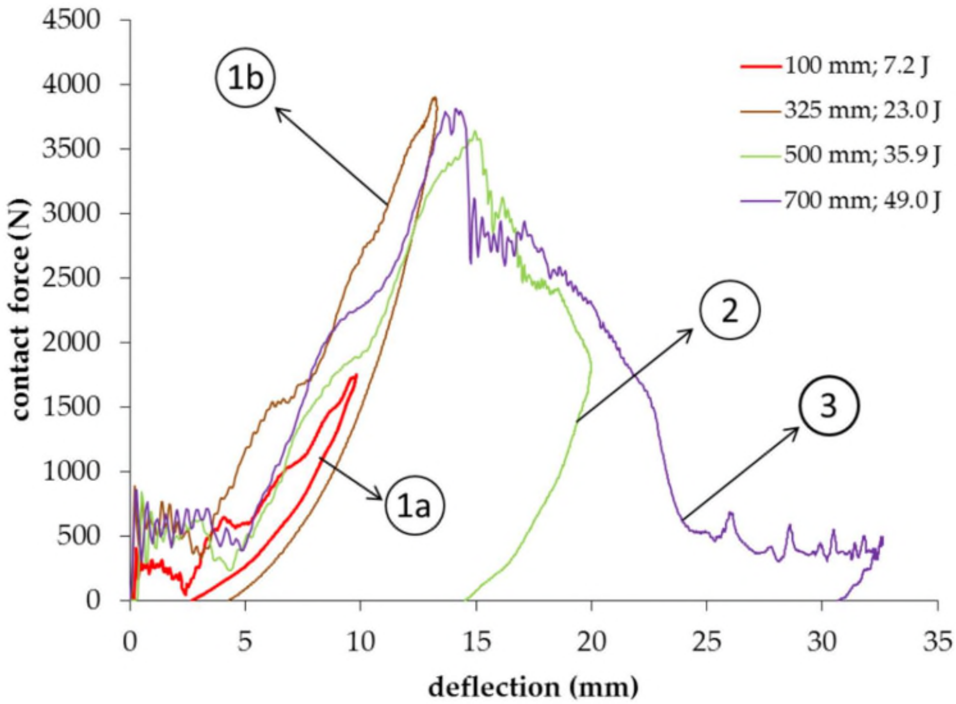

Figure2: *typical force-deflection curves extracted from master curve*

- at an impact energy of around 23 J (curve 1b in Figure 2), local damage starts to occur at the back side of the laminate at the point of impact. This could be called the damage initiation threshold. For impact energies higher than this one, the peak force remains constant: it is directly related to the bending- and shear resistance of the material. The deflection at peak load also remains constant, followed by a softening range increasing with impact energy, accompanied by a decreasing rebound. With increasing impact energy, additional damage will develop caused by fibre breakage at the backside due to local bending, and cracks will form under the impactor (curve 2 in Figure 2). An increasing fraction (over 50%) of the impact energy is absorbed. It is proposed to call this the damage development range;

- at an impact energy higher than 42 J, the impactor starts to penetrate in the laminate, corresponding to the penetration threshold. This is indicated by an increasing deflection (actually: the maximum displacement of the impactor) at constant low contact force caused by friction between the impactor and the specimen, before a very limited elastic rebound (curve 3). Finally, the impactor will not rebound anymore and will perforate the plate at the so-called perforation threshold.

3.2 Effect of varying parameters

Four series of tests are executed, while varying some parameters (Table 1): for series CSM-20, CSM-50 and CSM-70, the diameter of the impactor was varied from 20, over 50, to 70 mm in order to investigate its influence on the impact response; when comparing series CSM-70 with CSM-70-4, the influence of the thickness of the laminates is investigated. The test results are summarized in Tables 2 to 5. The drop height h, the impact velocity v_0, and the theoretical impact energy E_i are given in the first three columns. The next column represents the corrected impact energy, E_{ir}, taking into account the energy losses, amongst others, due to friction during the fall of the impactor. The remaining columns show the main impact characteristics, i.e. absorbed energy E_a, peak force F_{peak}, maximum deflection d_{max}, deflection at the peak force d_{peak}, and contact duration T.

Table 2: *results of CSM-20 series [21]*

speci-men	h (mm)	v_0 (m/s)	E_i (J)	E_{ir} (J)	E_a (J)	F_{peak} (N)	d_{max} (mm)	d_{peak} (mm)	T (ms)
1	50	0.99	3.9	3.7	1.2	1143	6.6	6.6	20.1
2	100	1.40	7.8	7.2	2.8	1750	9.8	9.8	19.6
3	200	1.98	15.5	14.2	6.6	2812	11.9	11.8	16.7
4	250	2.22	19.4	17.9	8.7	3208	13.3	13.2	16.5
5	325	2.53	25.3	23.0	11.5	3904	13.3	13.2	14.9
6	350	2.62	27.2	24.6	16.0	3782	14.5	13.8	16.2
7	400	2.80	31.1	27.9	22.5	3863	15.6	13.9	16.6

8	450	2.97	35.0	32.3	27.9	3739	17.4	14.0	17.3
9	500	3.13	38.8	35.9	32.4	3639	20.0	14.9	19.1
10	550	3.29	42.7	39.0	36.8	3325	22.2	13.9	22.2
11	575	3.36	44.7	40.5	37.2	3978	21.0	14.4	20.5
12	600	3.43	46.6	42.2	41.6	3776	24.6	13.7	29.2
13	700	3.71	54.4	49.0	48.6	3813	32.6	14.1	35.4
14	900	4.20	69.9	55.3	54.8	4235	-	13.4	-
15	1000	4.43	77.7	69.5	65.0	4115	-	13.8	-

Table 3: *results of CSM-50 series*

speci-men	h (mm)	v_0 (m/s)	E_i (J)	E_{ir} (J)	E_a (J)	F_{peak} (N)	d_{max} (mm)	d_{peak} (mm)	T (ms)
1	50	0.99	3.9	3.0	0.5	1093	6.7	6.7	20.2
2	100	1.40	7.7	6.1	2.4	1531	8.6	8.6	18.9
3	150	1.72	11.6	9.0	3.8	2026	10.9	10.9	17.8
4	250	2.22	19.3	14.7	7.0	2828	13.2	13.2	16.2
5	300	2.43	23.2	17.7	9.0	3149	14.5	14.5	15.6
6	350	2.62	27.1	20.6	12.0	3439	14.9	14.8	14.8
7	400	2.80	30.9	23.8	15.9	3470	15.2	14.9	14.8
8	450	2.97	35.0	26.8	19.3	3702	16.3	15.6	15.0
9	550	3.29	42.5	32.7	26.0	4079	17.9	16.8	14.9
10	650	3.57	50.3	38.3	31.6	4749	18.2	16.5	14.5
11	750	3.84	58.0	44.3	38.4	4520	19.9	17.2	15.1

Table 4: *results of CSM-70 series*

speci-men	h (mm)	v_0 (m/s)	E_i (J)	E_{ir} (J)	E_a (J)	F_{peak} (N)	d_{max} (mm)	d_{peak} (mm)	T (ms)
1	50	0.99	3.9	3.4	1.4	1129	5.9	5.9	18.5
2	100	1.40	7.7	6.8	3.2	1746	8.2	8.2	17.3
3	200	1.98	15.5	13.3	6.7	2764	10.7	10.6	15.5
4	250	2.22	19.3	16.6	8.1	3173	12.7	12.7	15.9
5	300	2.43	23.2	19.9	10.5	3630	12.9	12.7	14.6
6	350	2.62	27.1	23.0	12.4	3959	13.5	13.5	14.3
7	400	2.80	30.9	26.3	14.7	4262	14.9	14.7	14.4
8	450	2.97	34.8	29.1	15.4	4617	15.4	15.3	14.0
9	550	3.29	42.5	35.9	23.2	4788	17.2	16.6	13.8
10	650	3.57	50.3	43.1	33.9	5304	18.7	18.1	14.0
11	750	3.84	58.0	49.3	38.3	5828	19.2	18.5	13.4
12	850	4.08	65.7	55.5	45.1	6387	19.8	18.8	13.7

Table 5: *results of CSM-70-4 series*

speci-men	h (mm)	v_0 (m/s)	E_i (J)	E_{ir} (J)	E_a (J)	F_{peak} (N)	d_{max} (mm)	d_{peak} (mm)	T (ms)
1	50	0.99	3.9	3.5	1.6	943	10.1	10.0	25.8
2	100	1.40	7.7	6.8	3.4	1463	12.7	12.7	22.5
3	150	1.72	11.6	10.1	5.3	1924	14.4	14.3	20.5
4	200	1.98	15.5	13.4	7.4	2396	15.3	15.2	18.8
5	350	2.62	27.1	23.1	20.3	2557	21.0	16.4	23.3

The master curves, combining all individual force-deflection curves, as well as the corresponding energy-time curves, are depicted in Figures 3 to 6.

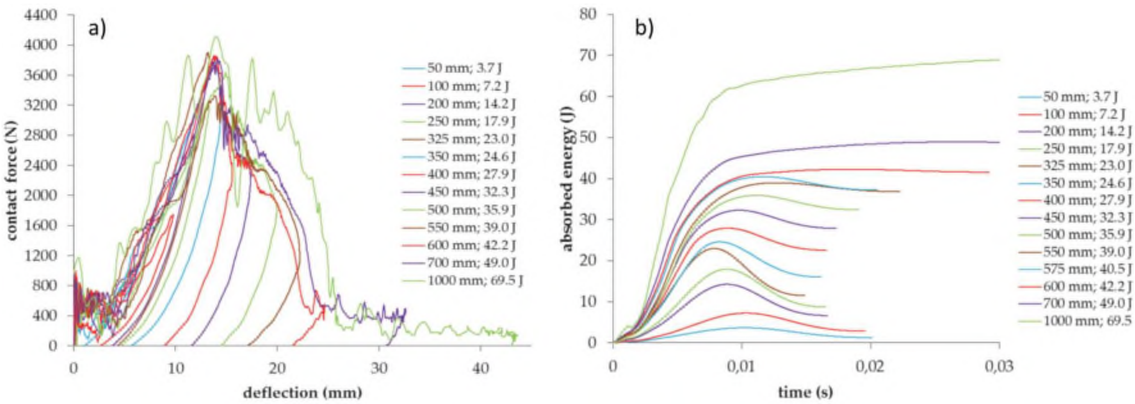

Figure 3: a) *master curve and b) energy-time curves of CSM-20 series*

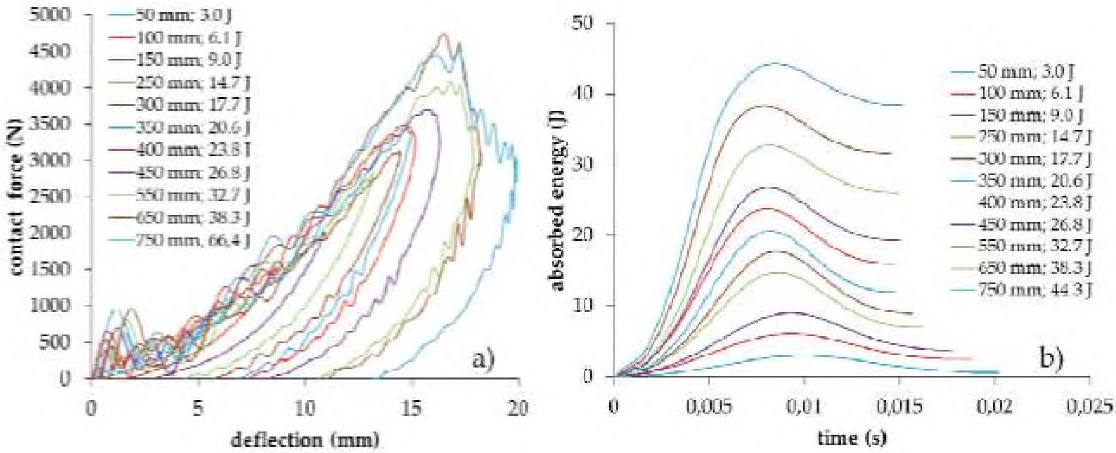

Figure 4: a) *master curve and b) energy-time curves of CSM-50 series*

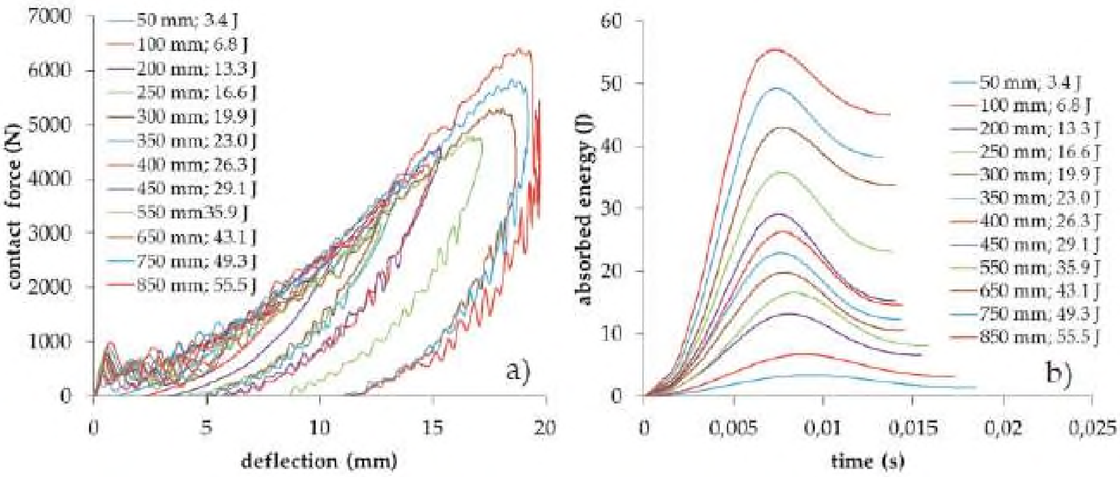

Figure 5: a) *master curve and b) energy-time curves of CSM-70 series*

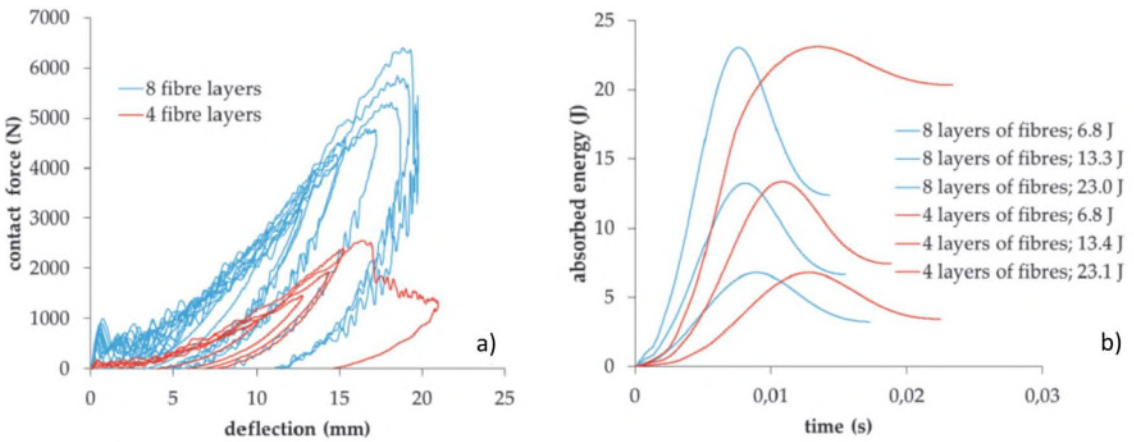

Figure 6: a) *master curve and b) energy-time curves of CSM-70-4 series*

The results from test series CSM-20 will be used as reference for the discussion, after which the influence of the varying parameters will be addressed. The following observations can be made for CSM-20, making use of the camera footage and visual observations after impact:

- regarding the energy-time curves, (Figure 3b), a clear change can be observed in the shape of the curves with increasing impact energy: in the first five tests (impact energy less than 23 J, up to curve 1b in Figure 2) a bell-shaped curve is observed. This indicates that the main part of the impact energy is elastically stored and returned to the impactor, causing it to rebound; thus only minor matrix crushing is observed besides indentation. The absorbed energy E_a is defined as the inelastically absorbed energy (final point of the curve), thus omitting the elastic energy used to rebound the impactor. Once impact energies higher than 23 J are applied, the curves start to flatten out. The elastic energy even approaches zero (horizontal tail of the curve) for the tests performed with an impact energy of 42.2 J and 49 J. This indicates that the extent of damage is increased dramatically. In the case of an impact energy of 69.5 J, perforation even takes place. This can be detected in the energy-time curve: the absorbed energy keeps increasing at a very low rate. This increase is however only due to friction between the impactor and the edges of the hole which is made in the plate. The energy absorption due to friction is therefore not taken into account for the energy absorption capacity.

Another clear trend in the energy-time curve can be found in the contact duration: this decreases first due to higher impact speed, but it starts to increase again when increasing energy absorption due to damage is observed;

- analogous to Liu's work [18], the threshold values for penetration and perforation can be calculated by using the energy profile (Figure 7). Penetration starts when the absorbed energy becomes equal to the impact energy, while the penetration threshold is the point where the absorbed energy again becomes lower than the impact energy. Liu suggests fitting a second order polynomial through all data points that are situated before reaching the equal energy line in Figure 7, in order to exactly determine the penetration threshold. A good correlation ($R^2 = 0.99$) is found and a penetration threshold of 42.5 J is calculated. It is not possible to exactly determine the perforation threshold from these tests, since only the last measuring point is situated again under the equal energy line. The perforation threshold is therefore assumed to lie in between these two measured points (55.3 J to 69.5 J);
- finally, the energy absorption efficiency can be calculated as the ratio between the area surrounded by the fitted curve and the impact energy-axis, and the area under the equal energy line up to the penetration threshold (see Figure 7). A value of 68.0% is obtained, which means that over the tested range of impact energies 68% of the impact energy can be absorbed by the tested material for the given impact conditions.

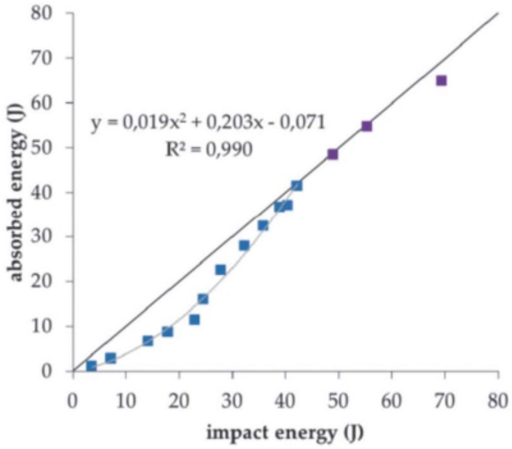

Figure 7: *energy profile CSM-20 series*

The most important impact characteristics of all series are summarised in Table 6. The peak force is given as an average value of the maximum forces of the curves that showed local damage. Its standard deviation, which is around 5 %, is also given in between brackets, except for CSM-70 where only one measurement is available.

Table 6: *comparison between results obtained from different test series*

series name	F_{peak}(N)	Damage initiation threshold (J)	Penetration threshold (J)	Energy efficiency coefficient (%)
CSM-20	3758 (189)	23.0	42.5	68.0
CSM-50	4634 (162)	20.6	56.0	79.2
CSM-70	6387	29.0	75.8	77.8
CSM-70-4	2477 (114)	15.5	26.6	75.0

The following observations can be made from the measurements (Figures 3 to 6, Tables 2 to 5) and computed impact characteristics (Table 6), together with the camera footage:

- the type of occurring local damage remains the same for all tested impactor sizes: after indentation, the damage mechanisms are local crushing and fibre-matrix debonding or delamination; further damage is caused by fibre breakage at the non-impacted side due to bending. However, larger impactor sizes lead to higher impact forces: the peak force and the penetration threshold are nearly doubled for an increase of impactor diameter from 20 mm to 70 mm. At the same time, matrix cracking becomes more globally distributed over the test plates. Furthermore, the energy efficiency is higher for the larger impactor sizes, since the damage development stage in the energy profile is larger: with the investigated impact energies, the energy-time curves remain bell-shaped (Figures 4 and 5), indicating that it was even impossible to reach the penetration threshold for impactor sizes of 50 mm and 70 mm; the values in Table 6 are obtained by extrapolation, following the procedure of Figure 7 which is on the conservative side since the real value is in between this value and the one next to it with higher impact energy;

- the effect of decreasing the laminate thickness is as expected: the peak force as well as the range of indentation and the penetration threshold decrease. However, the energy efficiency does not seem to be influenced by the thickness. This implies that in case of a given material combination, different impact energies can be absorbed with a constant efficiency by only adapting the thickness. However, when the peak force is a crucial design parameter, the situation becomes more complex: the peak force is found to increase more than linearly with thickness, due to the quadratic relation between elastic stresses and thickness. Finally, the matrix cracking density over the whole plate is found to be larger for thinner plates because of higher global deflections.

4. Comparison with polymer matrix composites

In general, the test results for IPC-TRC composites are qualitatively very similar to those reported for PMCs [18,19,23,24]. The shape of TRC and PMC master curves is comparable: above a critical impact energy, a constant peak force is reached and the subsequent unloading part exhibits two different stages: a first stage in which local damage is caused by the impactor, and a second in which the excess energy is returned to the impactor resulting in a rebound. The damage phenomena are however slightly different, indicated by the absence of closed curves for TRC. This is due to the low tensile strength of the cementitious matrix, leading to matrix damage and thus residual deflection from a relatively low impact energy on.

In order to situate the results obtained on the impact characteristics of IPC-TRC laminates in a broader context and to compare with PMC, a short overview of several experimental investigations from literature, based on the data given in Table 7, is provided in this section. The examples that are given below are chosen because their similarity in testing procedure and interpretation methodology with the ones that were applied in this work. Nevertheless, the test configurations are not equal for all cases, which complicates the interpretation. The specimen dimensions, the impactor diameter Φ_i and the fibre reinforcement architecture are presented in the first three columns of Table 7, followed by the computed parameters damage initiation threshold E_{dmg}, penetration threshold E_{pen}, perforation threshold E_{per} and energy efficiency coefficient η_E, as defined above. The first row of Table 7 contains the results for the glass fibre reinforced IPC composites from series CSM-20, the following ones results from literature on PMC.

Table 7: *comparison between TRC and PMC composites*

material	dimensions (mm)	$Ø_i$ (mm)	fibre arch.	E_{dmg} (J)	E_{pen} (J)	E_{per} (J)	η_E (%)
CSM-20	250x250x4.0	20	CSM	23.0	42.5	69.5	68.0
glass/epoxy *[23]*	270x270x4.0	19	woven	15.0	-	-	-
carbon/epoxy *[23]*	270x270x2.8	19	UD	30.0	-	-	-
glass/polyester *[24]*	100x100x4.0	10	UD	10.0	30.0	32.3	-
glass/polyester *[24]*	100x100x4.0	10	woven	15.0	40.0	50.0	-
glass/epoxy *[18]*	125x100x3.2	12.5	crossply	-	38.0	45.5	-
glass/epoxy *[19]*	125x125x6.3	12.5	crossply	-	127.9	143	76.1

It is clear from Table 7 that the reported specimen dimensions, as well as the size of the impactor, are not equal in all cases. It was observed above that an increasing impactor diameter causes the threshold values to be shifted to higher energies as a consequence of the larger contact area. On the other hand, the impactor size did not have an unambiguous effect on the energy absorption efficiency. A similar trend was reported by Liu [19]. Consequently, results for impactors with a similar size should be compared. On the other hand, the plate thickness obviously influences the force-deflection curves and the damage threshold values, but was found to have no significant effect on the energy absorption efficiency. For a good comparison of the results, the thickness should thus be similar except for the efficiency parameter. The effect of changing dimensions of the specimens has not been investigated in this work. Given the results that were discussed earlier, which clearly showed that the damage is occurring mainly locally, it can be assumed that the in-plane specimen dimensions do not have a significant effect on the energy absorption as long as the impact damage is local and does not reach to the boundaries.

Hosseinzadeh et al [23] investigated glass and carbon fibre reinforced epoxy laminates with different thicknesses (4.0 mm for glass/epoxy and 2.8 mm for carbon/epoxy). The specimen dimensions of the glass/epoxy specimens as well as the used impactor are very similar to those used in this work: specimens with dimensions 270 mm by 270 mm were clamped at 4 edges and impacted using a hemispherical impactor with a diameter of 19 mm. The mass of the impactor was also similar (5.5 kg). The damage initiation energy of the CSM-20 series (23 J) was found to be higher than the values reported by Hosseinzadeh et al for glass/epoxy composites, but lower than for carbon/epoxy composites (30 J) with a thickness of only 2.8 mm. Finally, it should be noted that the values reported by Hosseinzadeh et al are obtained on either woven or UD fabrics, which are assumed to perform better than CSM reinforcements due to the long fibre length.

Damage initiation thresholds are reported by Evci and Gülgeç [24] for woven and UD glass fibre reinforced polyester. Taking into account the smaller impactor size (diameter 10 mm) compared to the one used for the CSM-20 series, the damage initiation threshold can again be considered as comparable. Evci and Gülgeç also report penetration and perforation thresholds for these materials. Again, taking into account on one hand the smaller diameter of the impactor and on the other hand the more than double fibre volume fraction, the results can be considered as comparable with those obtained for the CSM-20 series.

It is more difficult to compare the results reported by Liu [18,19] to those obtained within this work, due to the differences as well in specimen thickness, impactor diameter and fibre architecture. Nevertheless, the reported values are still in the same order of magnitude when taking into account these differences and their effect on the threshold values.

Overall, it can be stated that the behaviour of IPC-TRC composites under low velocity impact as tested in a drop weight impact test, is very similar to that of PMCs. Taking into account several differences in the test configurations, all threshold values as well as the energy absorption efficiency were observed to be situated in the same order of magnitude. It can therefore be concluded that the low velocity impact performance of IPC-TRC composites can be characterised well with Liu's energy profiling method, and that IPC-TRC composites show a similar potential as PMCs for structures that can be subjected to accidental loadings.

5. Conclusions

The results obtained by drop weight impact testing of textile reinforced cement laminates reinforced with chopped strand glass fibre mats, allow the following conclusions to be drawn:

- Drop weight impact behaviour of textile reinforced cement laminates can be quantitatively described by the energy profiling technique, which has been proposed for polymer matrix composites [19]. The load-deflection curves for different impact energies show a mountain-like shape with a common master curve: a first loading stage up to the peak force is followed by a stage of descending force, first with increasing deflection resulting from local damage development, and secondly with decreasing deflection indicating rebounding of the impactor, unless perforation takes place.
- The observed damage mechanisms are similar to those of polymer matrix composites. In the first stage, local matrix crushing and indentation occur, while in the second stage fibre-matrix debonding and delamination occur, followed by fibre failure at the non-impacted side.
- The master curves as well as the energy-time curves and energy profiles are comparable to those for polymer matrix composites. The numerical values reported here for damage initiation threshold (23 J), penetration threshold (42 J), perforation threshold (69 J) and energy efficiency (75%) compare favourably with those from similar polymer matrix composites. A difference however is the absence of closed load-deflection curves due to early damage in the brittle

cementitious matrix. This implies that the impact is almost never fully elastic, although the absorbed energy in the ascending stage of loading is quite small.

- Changing the impactor size influences the peak force and the penetration threshold, which are nearly doubled for an increase of the impactor diameter from 20 mm to 70 mm. Also the energy absorption efficiency increases with larger impactor diameter. This implies that the investigated IPC-TRC laminates will perform better when subjected to larger impacting bodies.
- In case of a given material combination, different impact energies can be absorbed with a constant efficiency by only adapting the thickness. If however the peak force is a crucial parameter, the situation becomes more complex: the peak force is found to increase more than linearly with thickness, due to the nonlinear relation between stresses and thickness.

Acknowledgements

The authors gratefully acknowledge the financial support of the Research Foundation-Flanders (FWO) (Project N° G.0114.07N), and of the Government Agency for Innovation by Science and Technology (IWT-Vlaanderen).

References

[1] M.O.W. Richardson, M.J. Wisheart, Review of low-velocity impact properties of composite materials, Composites Part A, 27A, 1996, p. 1123-1131

[2] A.E. Naaman, H.W. Reinhardt, High performance fiber reinforced cement composites HPFRCC-4: International workshop Ann Arbor, Michigan, June 16-18, 2003, Cement and Concrete Composites, 2004, 26, 6, p. 757-759, DOI 10.1016/j.cemconcomp.2003.09.001.

[3] A.E. Naaman, H.W. Reinhardt, Proposed classification of HPFRC composites based on their tensile response, Materials and Structures, 2006, 39, p. 547-555, DOI 10.1617/s11527-006-9103-2.

[4] W. Brameshuber (ed.), RILEM Report 36: State-of-the-Art report of RILEM Technical Committee 201-TRC: Textile Reinforced Concrete, RILEM Publications S.A.R.L., 2006, 273 pp.

[5] W. Brameshuber (ed.), RILEM Proceedings 75: 2nd ICTRC Textile Reinforced Concrete: Proceedings of the International RILEM Conference on Material Science (MatSci) Volume I, RILEM Publications S.A.R.L., 420 pp.

[6] B. Mobasher, Mechanics of fiber and textile reinforced cement composites, CRC Press, 2012, 451 pp.

[7] T. Triantafillou (ed.), Textile fibre composites in civil engineering, Woodhead Publishing series in civil and structural engineering, Elsevier, 2016, 441 pp.

[8] J. Van Ackeren, J. Wastiels, Tensile behaviour of different high performance fibre reinforced cements, Proceedings of Brittle Matrix Composites 10, ed. A.M. Brandt et al, Woodhead Publishers, Warsaw, 2012, p 145-154.

[9] O. Remy, J. Wastiels, High performance textile reinforced cements: tensile hardening behaviour and modeling, Proceedings of CCC2008, Challenges for Civil Construction, eds. Torres Marques et al, FEUP, Porto, 2008, 10 pp.

[10] F. de Andrade Silva, M. Butler, V. Mechtcherine, D. Zhu, B. Mobasher, Strain rate effect on the tensile behaviour of textile-reinforced concrete under static and dynamic loading, Materials Science and Engineering A, 528, 2011, p 1727-1734.

[11] Y. Yao, A. Bonakdar, J. Faber, T. Gries, B. Mobasher, Distributed cracking mechanisms in textile-reinforced concrete under high speed tensile tests, Material and Structures, 49, 2016, p 2781-2798, DOI:10.1617/s11527-015-0685-4

[12] D. Zhu, A. Peled, B. Mobasher, Dynamic tensile testing of fabric-cement composites, Construction and Building Materials, 25, 2011, p385-395, DOI:10.1016/j.conbuildmat.2010.06.014

[13] D. Zhu, M. Gencoglu, B. Mobasher, Low velocity flexural impact behavior of AR glass fabric reinforced cement composites, Cement & Concrete Composites, 31, 2009, p 379-387, DOI:10.1016/j.cemconcomp.2009.04.011

[14] M. Gencoglu, Effect of fabric types on the impact behavior of cement based composites in flexure, Materials and Structures, 42, 2009, p 135-147, DOI:10.1617/s11527-008-9373-y

[15] V. Dey, A. Bonakdar, B. Mobasher, Low-velocity flexural impact of fiber-reinforced aerated concrete, Cement & Concrete Composites, 49,2014, p 100-110, DOI:10.1016/j.cemconcomp.2013.12.006

[16] V. Dey, G. Zani, M. Colombo, M. Di Prisco, B. Mobaher, Flexural impact response of textile-reinforced aerated concrete sandwich panels, Materials and Design, 86, 2015, p 187-197, DOI:10.1016/j.matdes.2015.07.004

[17] ASTM D7136/D7136M, Standard Test Method for Measuring the Damage Resistance of a Fiber-Reinforced Polymer Matrix Composite to a Drop-Weight Impact Event, 2007, pp. 16, ASTM

[18] D. Liu, B.B. Raju, X. Dang, Impact perforation resistance of laminated and assembled composite plates, International Journal of Impact Engineering, 24, 2000, p. 733-746.

[19] D. Liu, Characterization of Impact Properties and Damage Process of Glass/Epoxy Composite Laminates, Journal of Composite Materials, 38, 16, 2004, p. 1425-1442.

[20] S. Palanivelu, W. Van Paepegem, J. Degrieck, S. De Pauw, J. Vantomme, J. Wastiels, D. Kakogiannis, D. Van Hemelrijck, Low velocity axial impact crushing performance of empty recyclable metal beverage cans, International Journal of Impact Engineering, 38(7), 2011, p.622-636, DOI 10.1016/j.ijimpeng.2011.02.008.

[21] J. Wastiels, J. Van Ackeren, D. Van Nuffel, W. Van Paepegem, Impact behaviour of high performance glass fibre reinforced cement composite laminates, High Performance Fiber Reinforced Cement Composites – HPFRCC-7, Proceedings of the 7th Int. RILEM Workshop, Eds. H.W. Reinhardt et al, RILEM Publications, Bagneux (F), 2015, p 317-324.

[22] J. Blom, M. El Kadi, J. Wastiels, D.G. Aggelis, Bending fracture of TRC laminates monitored by acoustic emission: Influence of aspect ratio, Construction and Building Materials 70, 2014, p 370-378, DOI 10.1016/j.conbuildmat.2014.07.080.

[23] R. Hosseinzadeh, M. M. Shokrieh, L. Lessard, Damage behavior of fiber reinforced composite plates subjected to drop weight impacts, Composites Science and Technology 66, 2006, p. 61–68, DOI 10.1016/j.compscitech.2005.05.025.

[24] C. Evci, M. Gülgeç, An experimental investigation on the impact response of composite materials, International Journal of Impact Engineering, 43, 2012, p. 40-51, DOI 10.106/j.ijimpeng.2011.11.009.